International Journal of Applied Engineering Research ISSN 0973-4562 Volume 10, Number 18 (2015) pp 39509-39517

Analysis of Automotive Seat with Load and Vibration Transmitted due to Motor Position

Jae Ung Cho[1]

[1] *Division of Mechanical & Automotive Engineering, Kongju National University, 1223-24, Cheonan Daero, Seobuk-gu, Cheonan-si, Chungnam, 31080, Korea*
E-mail: jucho@kongju.ac.kr

Abstract
In this study, strength durabilities as a function of structures for loads acting on the seat motor and position changes as well as vibration were analyzed. In order to consider changes in vibration, analysis was conducted with a load equivalent to human weight was imposed while motor positions were varied, and amounts of deformation between 50Hz and 250Hz were observed. The durability verification of this brake design appears to be valid, since resonance is not normally considered to occur above this frequency even if passenger loads are high. If this study results are applied to the parts for an automotive car body, fatigue failures may be prevented while their durabilities may be predicted.

Keywords: Vibration, Motor Position, Natural Frequency, Critical Frequency, Equivalent Stress, Deformation

Introduction

Since reduction technologies for noise and vibration of vehicles are developing by leaps and bounds as human-oriented vehicle design and production technologies are developed throughout the entire automotive industry, seats have the closest relationship to passengers and are accounting for an important item in selection of vehicles by consumers.

As a result, a variety of methods are being attempted for evaluation and improvement. Since seats are an important final point where road vibration or engine vibration, etc., according to road conditions, is directly transmitted to passengers, it may be considered as an important element directly connected with riding comfort of a vehicle.

In addition, as consumers' complaints caused by abnormal sounds due to seat vibration tend to be increased, vibration noise characteristics of automobile seats need to be investigated. Therefore, vibration characteristics of seats produced when passenger loads are applied and when positions of a representative seat motors are moved, are analyzed in this study[1-8]. Also, vibration characteristics transmitted to the seat, natural vibration characteristics of the seat and shapes of problem vibration modes will be investigated through modal tests.

Therefore, diversified types of seat frames are available in the market, and transmitted vibration is varied with loads and positions of the seat motor. If the results of this study are combined for application to the arrangement operation for seat motors, it is considered to have great utilization for reviewing and predicting their structural strength and durability[9-12].

In this study, the modeling was carried out by CATIA V5R18 program and the structural analysis together with the vibration analysis was performed by using ANSYS program.

Study model

The size of this study seat model when viewed from the front is 530mm in length with 698.32mm and 786mm in width and depth, respectively. Shapes of the model were analyzed by using ANSYS after being modelled using CATIA with reference to the shapes of actual seats.

Mesh shapes for models 1 and 2 are shown in Figure 1(a) and Figure 1(b), respectively, where numbers of nodes and elements for model 1 were 42515 and 21942, respectively, while those for model 2 were 42515 and 21942, respectively. Table 1 shows the material property of this model.

(a) Model 1 **(b) Model 2**

Figure 1: Meshes of models

Table 1: Material property

Young's Modulus (MPa)	200000
Poisson's Ratio	0.3
Density (g/cm^{-3})	7.85
Tensile Yield Strength (MPa)	250
Tensile Ultimate Strength (MPa)	460

Structural Analysis

As boundary conditions for models 1 and 2 when loads were applied to the seat, the areas in contact with the floor were completely fixed as in Figure 2(a) and Figure 3(a), while the force of 700N of adult male's average load, which could be

actually applied in Z- direction, was imposed on the area in contact with the seat cover in Figure 2(b) and Figure 3(b). Also, as boundary conditions for models 1 and 2 when the motor was vibrated, the areas in contact with the floor were completely fixed as in Figure 2(a) and Figure 3(a), while the small force of 50 N, which could be actually applied in Z+ direction, was imposed on the periphery of seat motor in Figure 2(c) and Figure 3(c). Motor positions of models 1 and 2 are on the left and right in mutually opposite directions.

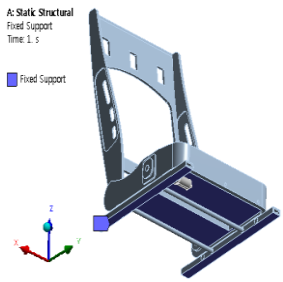

(a) Fixed support

(b) Force condition – weight

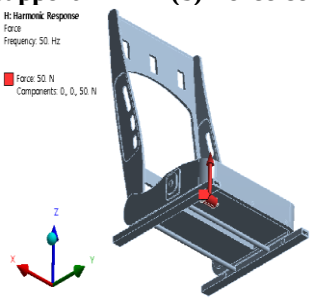

(c) Force condition - motor

Figure 2: Constraint condition of model 1

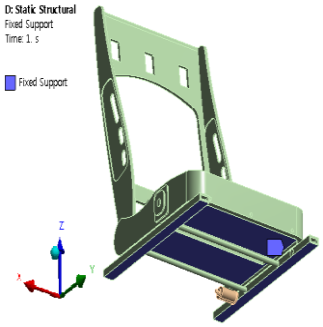

(a) Fixed support

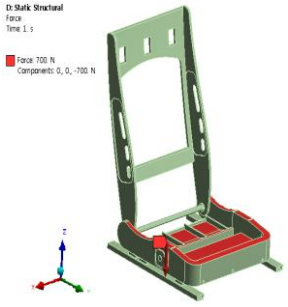

(b) Force condition – weight

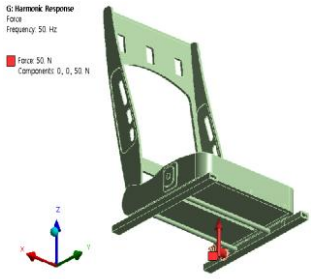

(c) Force condition - motor

Figure 3: Constraint condition of model 2

Figure 4 and Figure 5 in models 1 and 2 show equivalent stresses and maximum amounts of deformation when a static force was applied to the area in contact with the seat cover. Figure 4(a) and Figure 4(b) show maximum equivalent stresses for the areas in contact with the seat cover in models 1 and 2 to be 0.024107 MPa and 0.024022 MPa, respectively. As Figure 5(a) and Figure 5(b) show maximum amounts of deformation for upper part of the bumper in models 1 and 2, respectively, it may be seen to have been deformed to 1.9914×10^{-5} mm and 1.982×10^{-5} mm, respectively. In these figures, the structure strength of model 2 may be considered to be better since the amount of deformation for model 1 is larger than that for model 2. And, the structure strength of model 2 may be considered to be better indeed, since model 2 has a slightly smaller maximum stress than Mode 1.

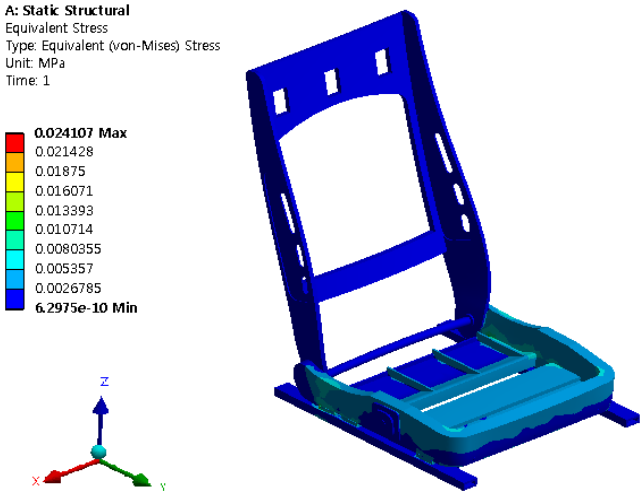

(a) Model 1

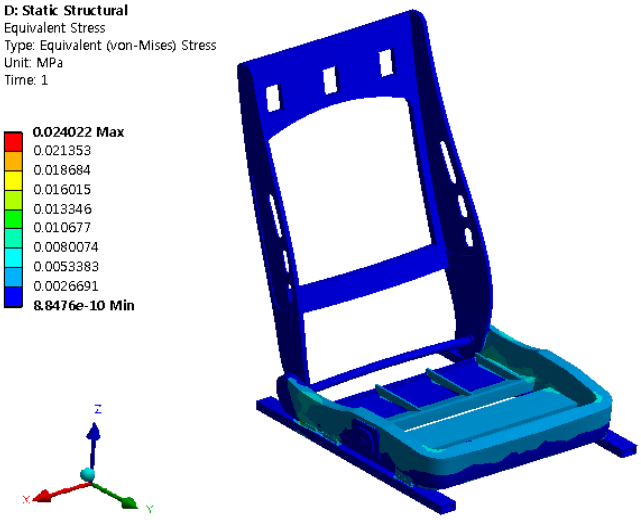

(b) Model 2

Figure 4: Equivalent stresses at structural analysis

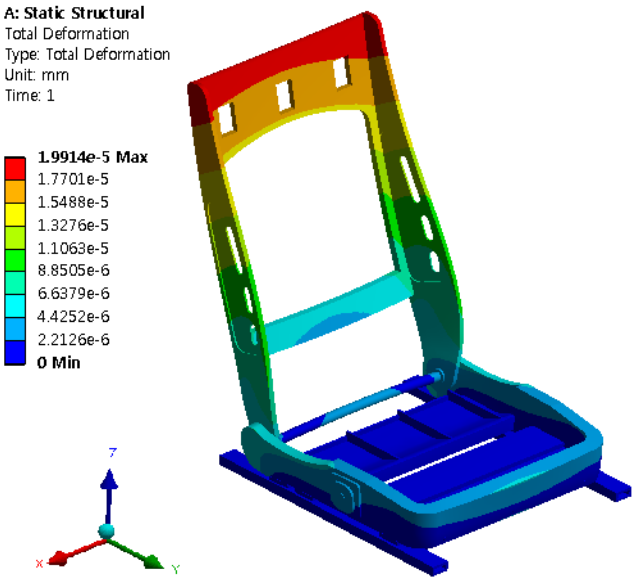

(a) Model 1

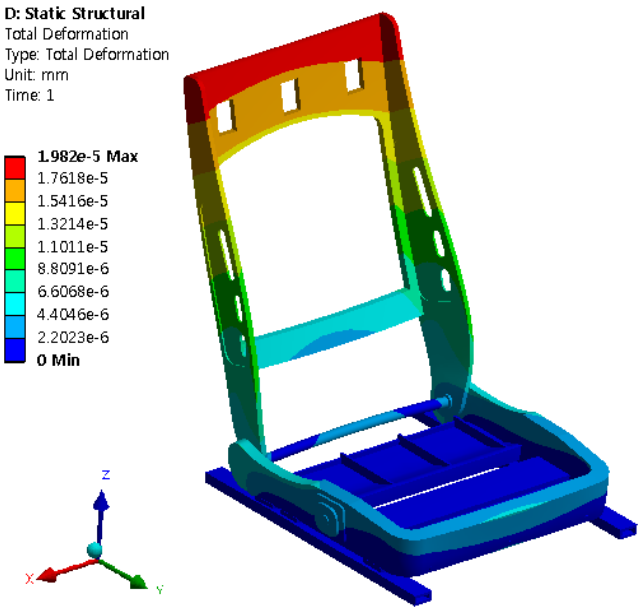

(b) Model 2

Figure 5: Total deformations in structural analysis

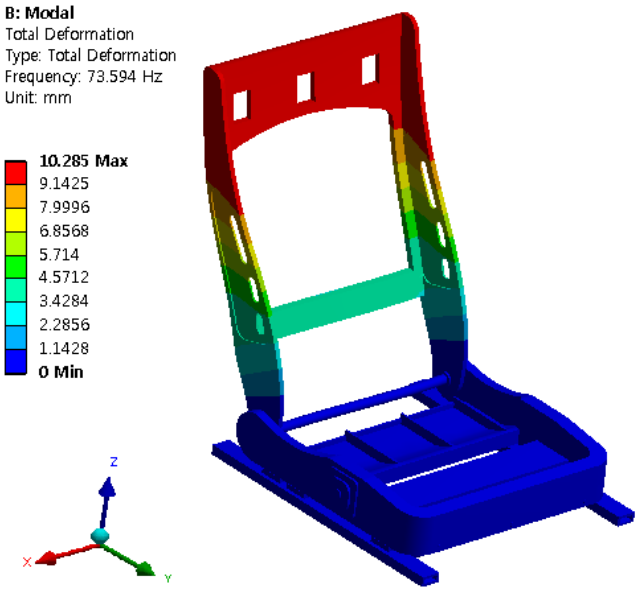

(a) Natural frequency at 1'st

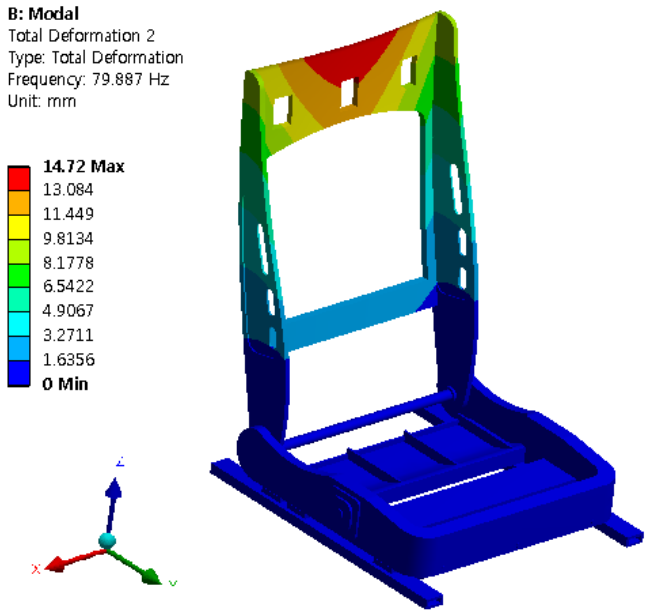

(b) Natural frequency at 2'nd

Vibration Analysis

Vibration analysis was performed to obtain natural frequencies of a seat, while frequencies and amounts of deformation in each mode for models 1 and 2 may be seen in Figure 6 and Figure 7. The frequencies and the amounts of deformation in each mode may also be shown in Table 2 and Table 3, where the maximum total amount of deformation in the 5'th mode of model 1 is 18.666 mm, while the amount of total deformation in the 5'th mode of model 2 is 590.15 mm showing the maximum amount of deformation. It may be predicted that responses in the 5'th mode of model 1 as well as the 5th mode of model 2 are the largest. At Table 2 and Table 3, the frequency in the 5th mode of model 1 is 227.52 Hz while that of model 2 is 227.53 Hz.

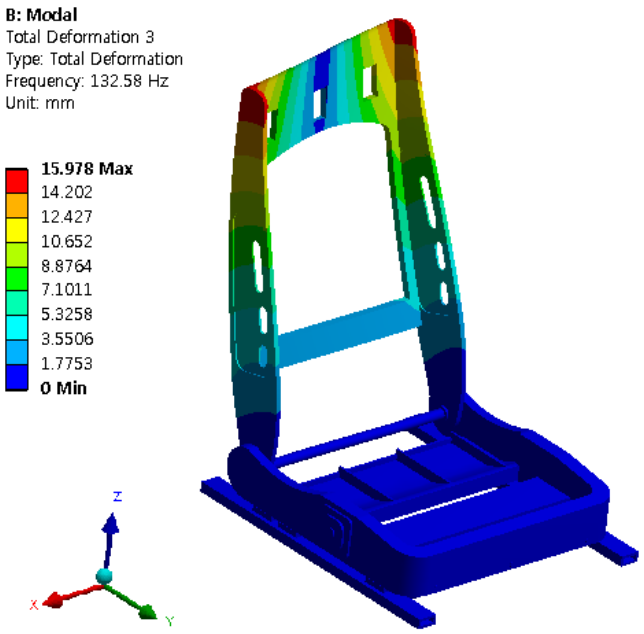

(c) Natural frequency at 3'rd

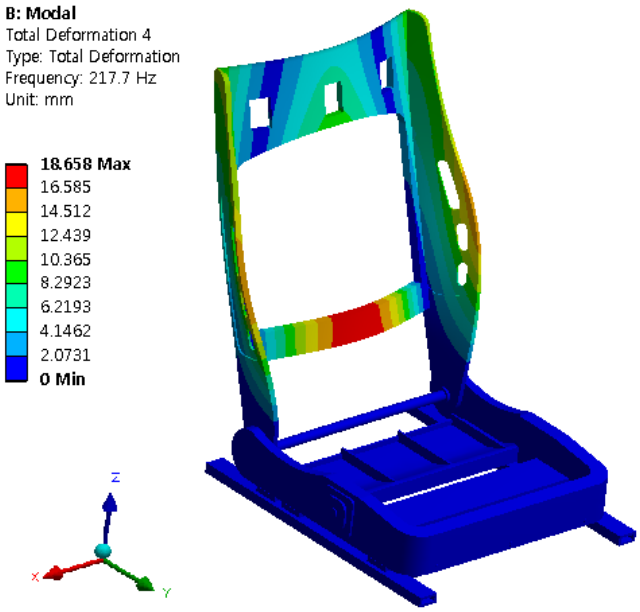

(d) Natural frequency at 4'th

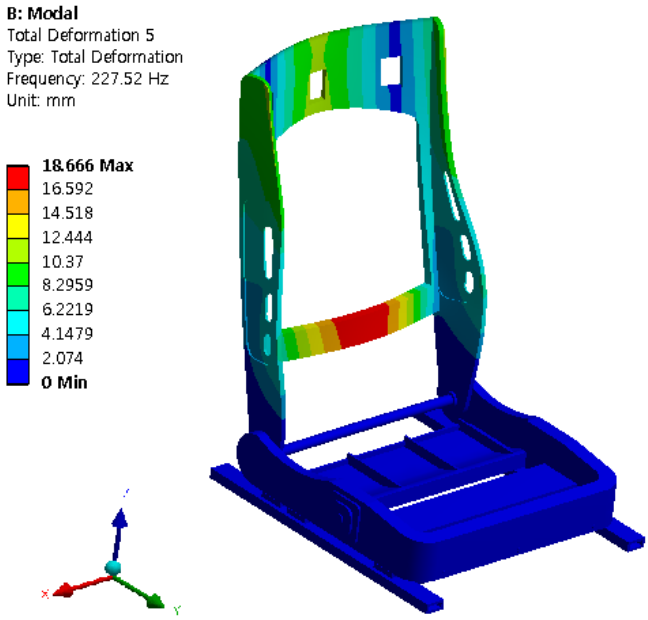

(c) Natural frequency at 5'th

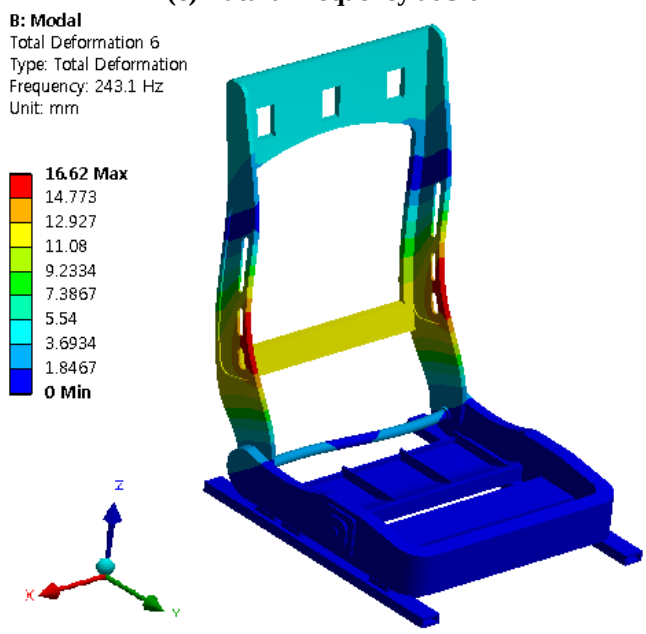

(d) Natural frequency at 6'th

Figure 6: Total deformation at natural frequencies of model 1

Even for passengers whose loads were actually small, neither the equivalent stress or the maximum stress was greatly reduced, nor the resonant frequency shown above exceeded in the case of resonance as well. Also, considering these results, verification results were shown that designs to improve riding comfort were possible since actual driving took place at lower frequencies than this although resonance occurred at 227.52 Hz and 227.53 Hz during a ride.

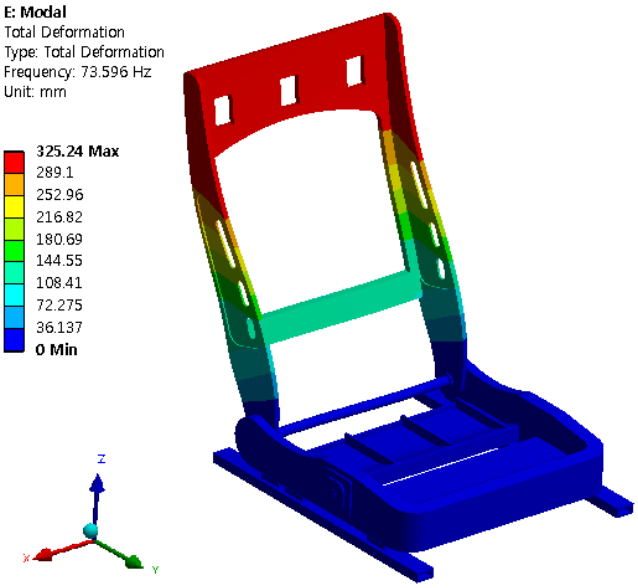

(a) Natural frequency at 1'st

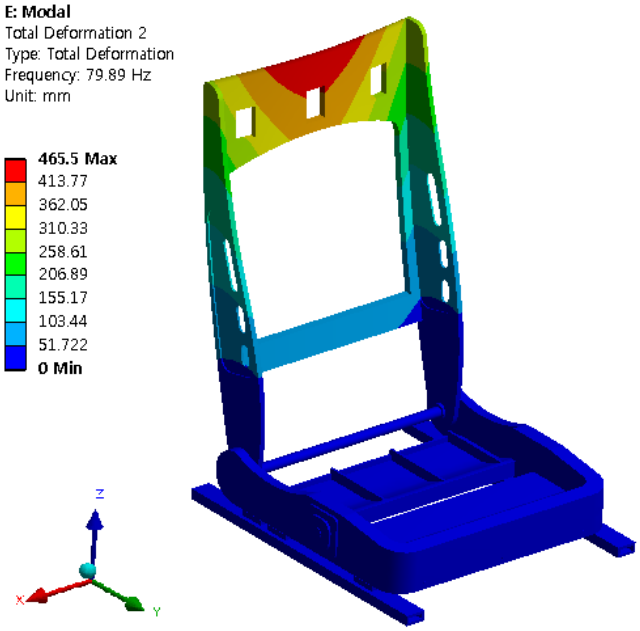

(b) Natural frequency at 2'nd

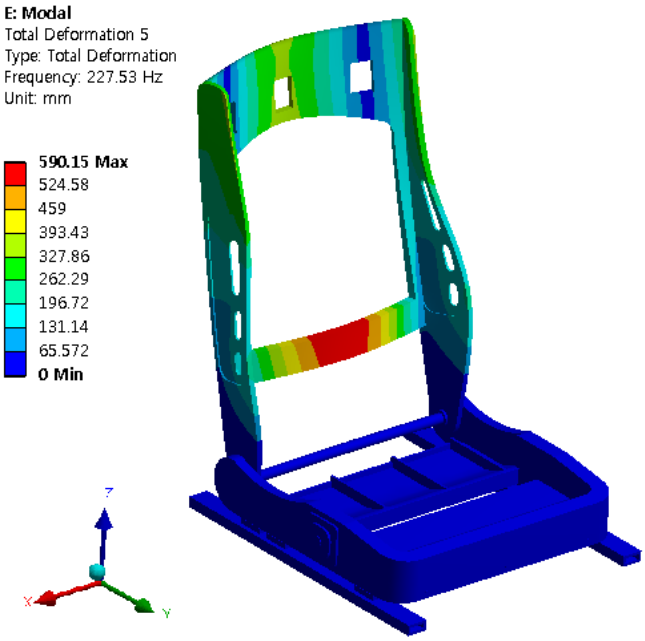

(c) Natural frequency at 3'rd

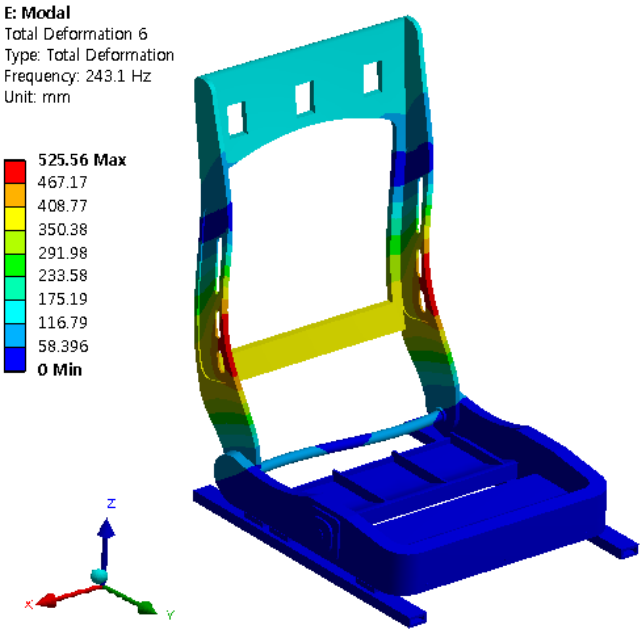

(d) Natural frequency at 4'th

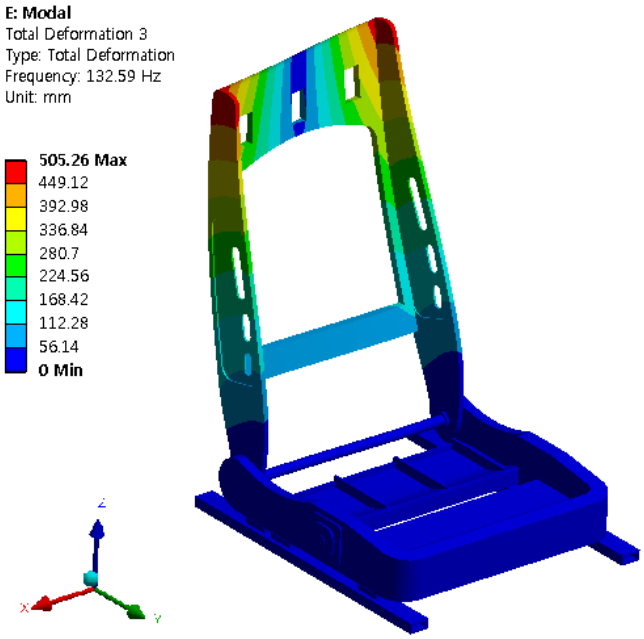

(e) Natural frequency at 5'th

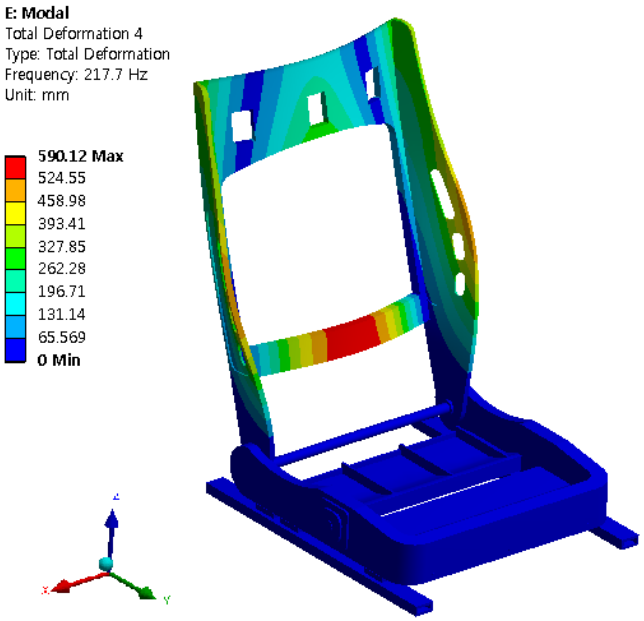

(f) Natural frequency at 6'th

Figure 7: Total deformation at natural frequencies of model 2

Table 2: Maximum total deformation and natural frequency per mode at model 1

	Frequency(Hz)	Total deformation(mm)
1'st mode	73.594	10.285
2'nd mode	79.887	14.72
3'rd mode	132.58	15.978
4'th mode	217.7	18.658
5'th mode	227.52	18.666
6'th mode	243.1	16.62

Table 3: Maximum total deformation and natural frequency per mode at model 2

	Frequency(Hz)	Total deformation(mm)
1'st mode	73.596	325.24
2'nd mode	79.89	465.5
3'rd mode	132.59	505.26
4'th mode	217.7	590.12
5'th mode	227.53	590.15
6'th mode	243.1	525.56

By actually imposing a constraint of 700 N in force to the face in contact with the seat cover in the same way as in Figures 2 and 3, an analysis was made for the harmonic vibration produced in the seat. The range of frequencies was set from 50 Hz to 250 Hz. Considering the previous results of modal analysis, resonance frequencies were affirmed according to the frequency domain occurring since the natural frequency for the 6'th mode was within the 250 Hz range.

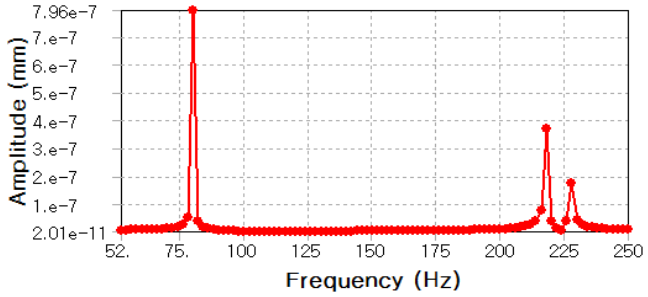

(a) Model 1

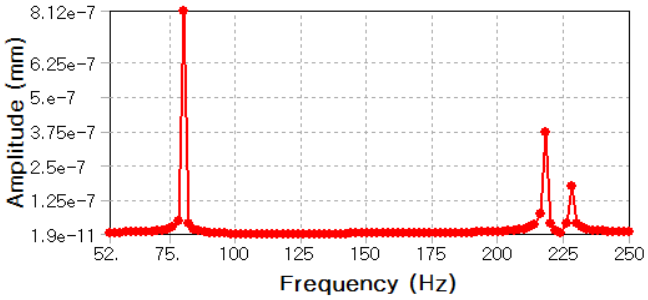

(b) Model 2

Figure 8: Frequency responses of amplitude displacements

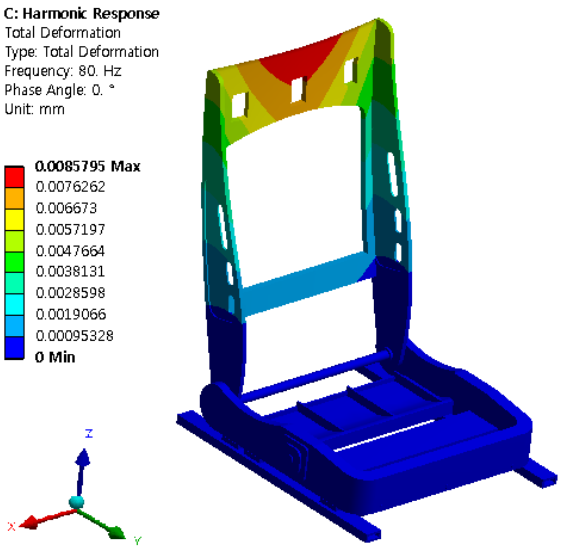

(a) At 80 Hz in model 1

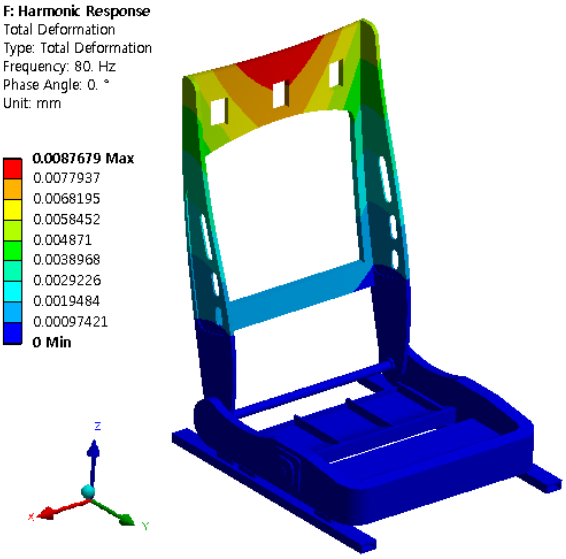

(b) At 80 Hz in model 2

Figure 9: Total deformation at critical frequencies

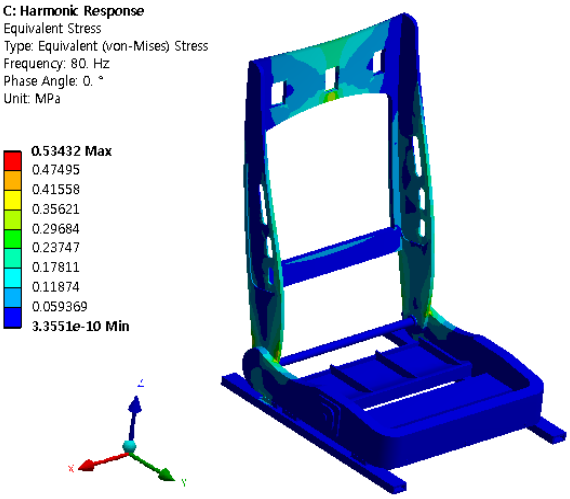

(a) At 80 Hz in model 1

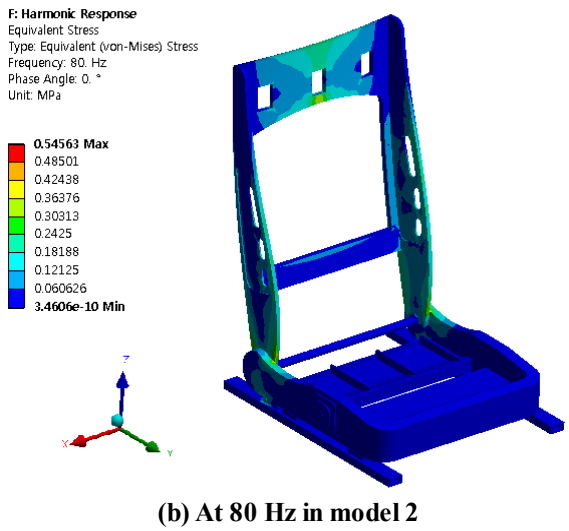

(b) At 80 Hz in model 2

Figure 10: Equivalent stresses at critical frequencies

As can be seen from Figure 8(a) and Figure 8(b) where amplitude displacement responses to frequencies were examined for models 1 and 2, model 1 showed a critical frequency at 80 Hz while model 2 showed it at 80 Hz. At such critical frequencies for models 1 and 2, the amplitude displacements can be seen to be generated as 7.96×10^{-7} mm and 8.12×10^{-7} mm, respectively. As durability of a model is improved, the higher the critical frequency, the durability may be considered to be the same since the critical frequency of model 1 is the same as that of model 2. Therefore, at the critical frequency of 80 Hz for models 1 and 2, practical total deformations and equivalent stresses were shown to be as shown in Figures 9(a), (b) and Figures 10(a), (b), respectively.

Likewise, the harmonic vibration when the motor was subjected to vibration was analyzed. Previously, in Fig. 2(c) and Fig. 3(c), a small force of 50N which could be actually applied in Z+ direction was imposed on a periphery of the seat motor. When the results of modal analysis were considered, resonant frequencies were affirmed in accordance with the frequency domain occurring since the natural frequency in the 6th mode was within the 250 Hz range. As can be seen from Figures 11(a), (b) where the amplitude displacement responses to frequencies were examined for models 1 and 2, model 1 showed a critical frequency at 80 Hz, while model 2 showed it at 244 Hz. From such critical frequencies for models 1 and 2, the amplitude displacements can be seen to be generated as 4.64×10^{-9} mm and 2.97×10^{-5} mm, respectively. As the result, the durability of model 2 may be seen to become more satisfactory than that of model 1 since the critical frequency of model 2 is higher than that of model 1. Consequently, at the critical frequencies of 80 Hz and 244Hz for models 1 and 2, respectively, practical total deformations and equivalent stresses for models 1 and 2 were shown to be as indicated in Figures 12(a), (b) and Figures 13(a), (b), respectively.

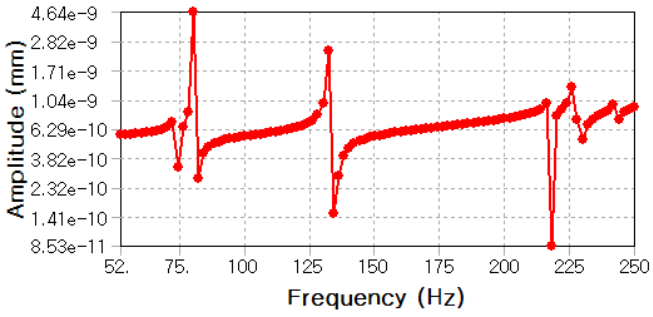

(a) Model 1

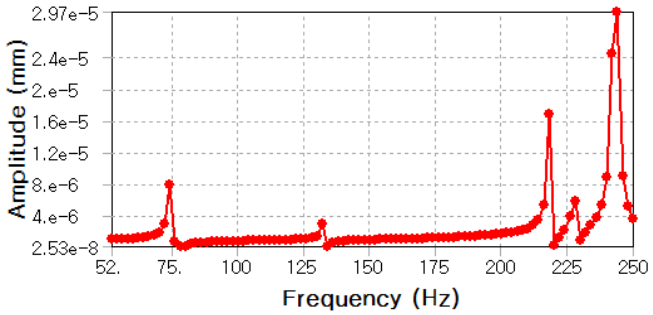

(b) Model 2

Figure 11: Frequency responses as amplitude displacements

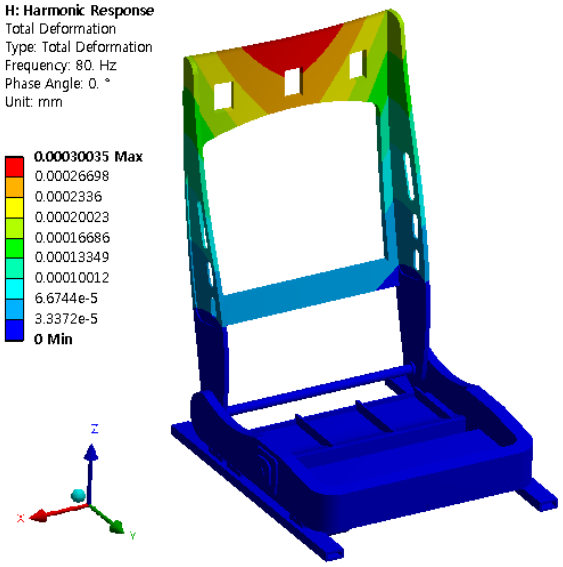

(a) At 80 Hz in model 1

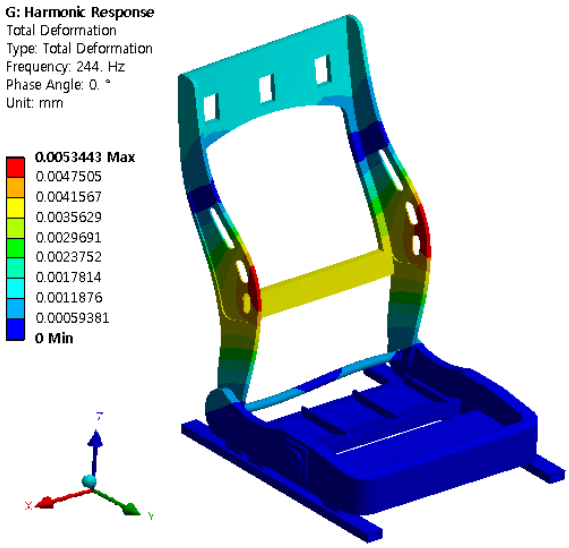

(b) At 244 Hz in model 2

Figure 12: Total deformation at critical frequencies

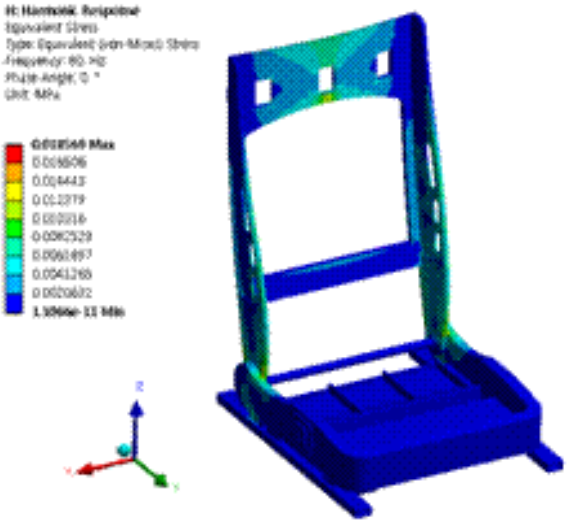

(a) At 80 Hz in model 1

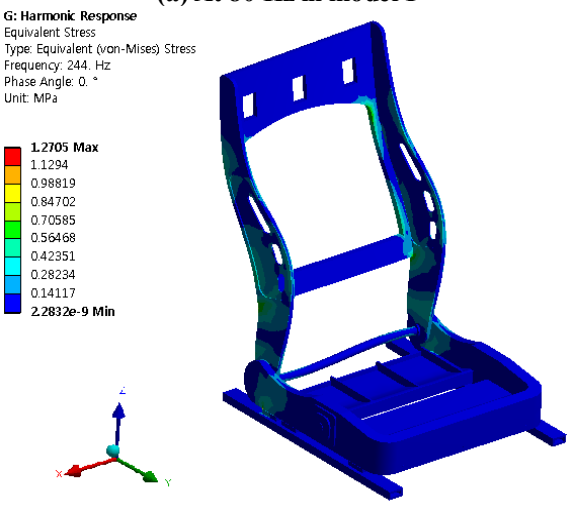

(b) At 244 Hz in model 2

Figure 13: Equivalent stresses at critical frequencies

Conclusions

In this study, strength durabilities as a function of structures for loads acting on the seat motor and position changes as well as vibration were analyzed. Study results therefore are as follows.

According to the structural analysis, the maximum equivalent stresses for model 1 and model 2 were shown to be 0.024107 MPa and 0.024022 MPa, respectively, while the amounts of deformation were shown to be 1.9914×10^{-5} mm and 1.982×10^{-5} mm, respectively, at a maximum. Model 1 can be seen to produce a slightly larger deformation than model 2. Also, it may be seen that natural frequencies of model 1 and model 2 occur within the range of 50 Hz to 250Hz, and the frequency in the 5'th mode of model 1 where deformation is actually easy and the possibility for occurrence of resonance appears to be high is 227.52 Hz while the frequency in the 5'th mode of model 2 is 227.53 Hz.

At frequency responses as a function of passenger loads, the maximum amplitude displacements for model 1 and model 2 at the same frequency of 80 Hz may be seen to be generated as 7.96×10^{-7}mm and 8.12×10^{-7} mm, respectively. When harmonic frequency responses are also considered as a function of position changes of the seat motor, it may be seen that the maximum amplitude displacements at 80 Hz for model 1 and at 244 Hz for model 2 are generated as 4.64×10^{-9} mm and 2.97×10^{-5} mm, respectively. The durability of model 2 can be seen to be better than that of model 1, since the durability is the more satisfactory, the higher the resonant frequency. Therefore, durability verification of this apparatus design appears to be valid, since resonance is not normally considered to occur above this frequency even if passenger loads are high. If this study results are applied to the parts for an automotive car body, fatigue failures may be prevented while their durabilities may be predicted.

Acknowledgments

This work was (partly) supported by Advanced Motor Parts Regional Innovation Center (AMP.RIC) of Kongju National University administered by MKE (Ministry of Knowledge Economy), Korea.

References

[1] Paweł, G., and Mariusz, L., 2015, "Computational model for friction force estimation in sliding motion at transverse tangential vibrations of elastic contact support," Tribology International, 90, pp. 455-462.

[2] Hu, H., Lu ,W.J., and Lu, Z., 2012, "Impact crash analyses of an off-road utility vehicle - Part II: Simulation of frontal pole, pole side, rear barrier and rollover impact crashes," International Journal of Crashworthiness, 17(2), pp.163-172.

[3] Acar, E., and Solanki K., 2009, "Improving the accuracy of vehicle crashworthiness response predictions using an ensemble of metamodels," International Journal of Crashworthiness, 14(1), pp.49-61.

[4] Cho, H. S., Cho, J. U., Kim, K. S., and Choi, D. S., 2013, "Structurally safe design of rear seat frame applied with high tension steel plate," International Journal of Digital Content Technology and its Applications, 7(12), pp.444-450.

[5] Erdem, A, and Kiran, S., 2009, "Improving the accuracy of vehicle crashworthiness response predictions using an ensemble of metamodels," International Journal of Crashworthiness, 14(1), pp.49-61.

[6] Zhan, J, Fard, and M., Reza, J., 2014, "A model to assess the comfort of automotive seat cushions," International Journal of Occupational Safety and Ergonomics, 20(3), pp.525-533.

[7] Shirsendu, D., and Amit, K., 2015, "Concept of an Electromagnetic Solar Based Power Drive for Automobile," IJAST, 76, pp.21-26.

[8] Yang ,Y., and Xu, H., 2010, "Finite Element Analysis of Power Spinning and Spinning Force for Tube Parts," IJAST, 20, pp.53-60.

[9] Zhang. J., Huang. X., Tian, D., and Wang, H., 2011, "CAE analysis and design modification for rear seat safety during vehicle frontal crash," Qiche Gongcheng/Automotive Engineering, 33(9), pp. 767-771.

[10] Nguyen, S. D., Nguyen, Q. H., and Choi, S. B., 2015, "A hybrid clustering based fuzzy structure for vibration control – Part 2: An application to semi-active vehicle seat-suspension system," Mechanical Systems and Signal Processing, 56-57, pp.288-301.

[11] Thakur, M., and Saikhedkar, N. K., 2013, "Behavioral Modeling and Simulation with Experimental Analysis of a Two Stroke Engine Using Nanosized Copper Coated Catalytic," IJAST, 59, pp. 97-112.

[12] Cho, J. U., 2015, "Vibration Analysis Due to Load Delivered to Automotive Seat and Motor Position," Advanced Science and Technology Letters, 108, pp. 14-18.